International Journal of Microscale and Nanoscale Thermal … ISSN: 1949-4955
Volume 4, Number 1

ONSET OF NUCLEATE BOILING AND CRITICAL HEAT FLUX WITH BOILING WATER IN MICROCHANNELS

R. R. Bhide[1], S. G. Singh[2], Vijay S. Duryodhan[1], Arunkumar Sridharan[1], and Amit Agrawal[1,*]

[1]Indian Institute of Technology Bombay, Powai, Mumbai, India
[2]Indian Institute of Technology, Hyderabad, India

ABSTRACT

This paper focuses on experimental determination of onset of nucleate boiling (ONB) and critical heat flux (CHF) at the microscales, and comparison of these with available correlations. The working fluid is deionised water and microchannel of four different hydraulic diameters: 65, 70, 107 and 125 μm, have been tested. Effect of hydraulic diameter (65-125 μm), mass flux (60-1410 kg/m^{2}s) and heat flux (0-910 kW/m^2) on ONB and CHF has been studied in detail. The heat flux for onset of nucleate boiling increases with hydraulic diameter and mass flux. The critical heat flux tends to increase with a decrease in hydraulic diameter and with increasing mass flux. The effect of surface roughness on CHF has also been tested to a limited extent; no clear change in the CHF value was observed upon changing the surface roughness by an order of magnitude. The empirical correlations tested in this study predict the experimental data to varying extent. These results may help better determine the lower and upper limits of heat flux while designing heat sink for electronic cooling.

Keywords: Two phase flow, ONB, CHF, Boiling incipience

NOMENCLATURE

Symbol used	Description	Units
A	Area	m^2
Cp	Specific heat of the fluid	J/kg-K
d_h	Hydraulic Diameter	m
H	Height of channel	m

* Corresponding author: Dr. Amit Agrawal, Department of Mechanical Engineering, Indian Institute of Technology Bombay, Powai Mumbai 400076, INDIA, Email: amit.agrawal@iitb.ac.in, Phone: +91-22-2576-7516, Fax: +91-22-2572-6875

h_{fg}	Latent heat of evaporation of fluid	J/kg
G	Mass flux	kg/m^2-s
L	Length in the microchannel	m
$\dot{m}$	Mass flow rate	kg/s
P	Power	W
ΔP	Pressure drop	mbar
q”	Heat flux	W/m^2
Q	Volumetric flow rate	m^3/s
T	Temperature	ºC
u	Velocity	m/s
W	Width of the microchannel	m
x	Quality	-
ε	Surface roughness	m
ρ	Density	kg/m^3
ρ_H	Homogenous Density	kg/m^3
υ	Specific Volume	m^3/kg
μ	Viscosity	cP
σ	Surface Tension	N/m
Re	Reynolds Number	-
Fr_H	Froude Number	-
We_H	Weber Number	-

Subscript	**Description**
w	Wall
sat	Saturation
in	Inlet
exit	Exit
cross	Cross-sectional
h	Heated
air	Ambient
supp res	Supplied Reservoir
chan	Channel
pred	Predicted
expt	Experiment
f	Fluid
g	Vapour
tp	Two phase
sp	Single phase
i,f	Frictional Pressure drop
a,f	Acceleration Pressure drop
avg	Average
fo	Fluid only
go	Vapour only

1. INTRODUCTION

In the recent past, there has been an increasing trend to use miniaturised systems. The development of fabrication techniques and the advances in semiconductor technology have led to the development of miniaturised electronic components. These devices need to be maintained below a certain temperature for efficient working. Due to increased storage capacity, faster performance, the heat to be dissipated from electronic components has increased considerably. It has been found that dissipating heat fluxes greater than 100 W/cm^2 using conventional air cooling would be difficult. The use of microfluidic devices to remove high heat fluxes is thus being widely researched as a viable alternative. Apart from cooling of electronic components, the micro-thermal-mechanical systems can be used in portable computer chips, radar and aerospace avionics components, and in microchemical reactors [1].

A large amount of work has been devoted to the study of fluid flow and heat transfer mechanisms in microchannels. Specifically, researchers have concentrated on the prediction of flow patterns [2-6], heat transfer characteristics [4-9] and instability [5, 10-12] in two phase flow in microchannel. Singh et al. [13] found a strong dependence of two-phase pressure drop on aspect ratio in rectangular microchannel, with a minimum at an aspect ratio of about 1.6. Singh et al. [5] have reported the pressure drop in a 109 μm hydraulic diameter trapezoidal cross-section microchannel over a wide range of inlet mass flow rate and heat flux values. The pressure drop was found to exhibit a maximum with a reduction in mass flow rate for a constant heat flux. With a subsequent reduction in mass flow rate, the pressure drop rises rapidly. Their comprehensive data is further analyzed in this paper. This work was extended by Bhide et al. [12] to study mean and r.m.s. of pressure drop in sub-hundred sized microchannels. They found a reduction in pressure instabilities with a reduction in hydraulic diameter and increase in wall roughness. See Agrawal and Singh [36] and Singh et al. [37] for a recent review on flow boiling in microchannel.

Onset of nucleate boiling (ONB) and critical heat flux (CHF) are important issues in the study of two phase flow, especially in the design of microchannel heat sinks. Onset of nucleate boiling marks the beginning of the region of improved heat transfer. Several researchers [25-27] have developed correlations to predict ONB for flow boiling in conventional scale flow passages. Basu et al. [33] performed subcooled flow boiling experiments on conventional scale passages fabricated using copper plate and nine zircalloy rod bundle. They developed a correlation for heat flux and wall superheat required for bubble inception, and suggested that these parameters are dependent upon mass flow rate, liquid subcooling, and contact angle. Also, they developed a correlation for nucleation site density which is primarily dependent upon the contact angle. Qu and Mudawar [34] performed experiments on parallel microchannels to measure the incipient boiling heat flux. They developed a model to predict the incipient boiling heat flux, accounting for the complexities of bubble formation along the flat and corner regions of a rectangular flow microchannel. They have also accounted for the likelihood of bubbles growing sufficiently large to engulf the entire flow area of a microchannel. Liu et al. [35] experimentally investigated the onset of nucleate boiling and developed an analytical model to predict important parameters such as incipience heat flux, bubble size, etc. during ONB.

CHF is the maximum heat flux that can be applied to the heater surface without causing permanent damage to the device and therefore represents the upper limit for heat transfer in

two phase flow. CHF is the outcome of events that cause a sudden appreciable decrease in the heat transfer coefficient of a surface on which boiling is occurring. However, the value of CHF is seldom reported in literature because it is rather difficult to obtain – more so at the microscales. Qu and Mudawar [14] found that CHF increases with mass flux but does not depend on the inlet temperature. They attributed this to the vapour back flow due to the parallel channel instability which negated the effect of liquid subcooling. They developed a correlation from the data for water in rectangular microchannels and the data for R-113 in circular mini/ microchannel heat sinks available from their earlier study. The developed a correlation as a function of vapour and liquid densities, channel dimensions, and Weber number. Jiang et al. [7] carried out experiments for calculation of the CHF in microchannels of 40 and 80 μm hydraulic diameters. Although they did not carry out flow visualisation study, from the temperature data collected they postulated that the boiling mechanism may be different for smaller microchannels. They observed different trends in the streamwise temperature profile for microchannels of 40 μm and 80 μm hydraulic diameters at CHF conditions. For the case of 40 μm channel, they postulated that the bubble nucleation activity is suppressed and boiling takes place through forced convection vaporization. They concluded that the bubble dynamics mechanism is very different and that the mechanism of bubble growth may be completely suppressed in smaller microchannels. Some studies with working fluid other than water are also available; for example, Ribatski et al. [15] worked with refrigerants (R-134a and R-245fa) while Lee and Mudawar [16] used a dielectric fluid (HFE 7100). Following important points are noted from the CHF data reported in the literature: (i) The exit quality at which CHF occurs decreases by about 1.7 times for the two-fold increase in mass flux, and (ii) the correlations of Katto, Sudo and Mudawar suggest that CHF in microchannels is a weak function of inlet subcooling. However, the correlation of Mishima shows substantial dependence on inlet subcooling. CHF studies for refrigerant-123 are available in Refs. [17-19].

Kosar [20] used the annular flow model of Qu and Mudawar and mass deposition coefficient of Patankar and Puranik [21] to predict the value of CHF for both water and refrigerant. The model predicts the experimental data for water with a mean absolute error of 28.9%, and in most cases the model predicted a larger value of CHF than experimentally determined. The discrepancy was attributed to either presence of parallel channel instability which leads to pre-mature CHF, or large thickness of the microchannel wall which tends to make the wall temperature uniform thereby delaying CHF. Kuan and Kandlikar [18] investigated the effect of flow instabilities in six parallel rectangular microchannels, each having a cross-sectional area of $1054 \times 157\ \mu m^2$. They postulated that the ratio of evaporation momentum to surface tension force is an important parameter. This formed the basis of theoretical analysis of flow boiling phenomena and theoretical CHF model is proposed using these underlying forces to predict CHF in microchannels. The proposed correlation agrees with the experimental data with a mean average error of 8.2% for water. Recently, Roday and Jensen [19] compared the data for water and R-123 with existing micro/microchannel correlations. They found that existing large-sized correlations do not predict CHF in microchannels. Therefore, they developed a new correlation in low-flow subcooled boiling situation from their experimental data. Chandraker et al. [22] pointed out that the mechanism of CHF even at the conventional scales is not well understood and needs careful investigation.

It is clear from the literature survey that very few experimental studies have reported the value of CHF. This study intends to partly fill this gap by providing data-points for four

different size microchannels and at different heat flux values. The obtained values are compared with available correlations. CHF is detected in the experiments by a sudden rise in temperature of the heater surface due to a decrease in the heat transfer coefficient. Literature available on ONB suggest that the bubble dynamics in microchannel differs from that in conventional scale passages, and therefore has an even greater impact on performance of microchannel based heat sinks. Also, it has been observed that there is lack of available data on effect of microchannel surface condition on ONB. Hence, data for the onset of boiling is also obtained and compared with existing empirical correlations.

2. EXPERIMENTAL SETUP AND DATA REDUCTION

2.1. Fabrication of Microchannels

The fabrication of microchannels is done in-house at IIT Bombay. The microchannels are fabricated on a 2-inch, 275 ± 25 μm-thick, p-type, <100> double-side-polished silicon wafer. Trapezoidal microchannels of dimension 77 μm × 270 μm (at the top) × 20mm (L) (yielding a width of 158 μm at the bottom and a hydraulic diameter of 107 μm) are fabricated by a sequence of process steps. The size of reservoir at the two ends of the microchannel is 6 mm × 6 mm. Note that other hydraulic diameter trapezoidal microchannels such as 65 μm, 70 μm and 125 μm have also been employed in this work. The surface roughness as determined using profilometer was found to be less than 0.1 μm for all microchannels (other than for 70 μm channel). The sealing of the microchannels with a quartz plate is a crucial step in fabrication and special care was taken to avoid leakage. A detailed description of microchannel fabrication is provided elsewhere [5, 6, 12, 13].

A multi-film stack of Ti-Pt is used to fabricate the microheater for controlled heat flux generation. Fabrication and characterization details are again mentioned in Ref. [13]. The resistance of the fabricated micro heater is found to be 445 ohm at room temperature.

The amount of subcooling at the inlet varies between 15 to 45 ^{0}C, while the exit pressure is atmospheric (1 bar). The heat loss was calculated using the standard technique of supplying power to the test section without any flow of water. All the heat supplied in this case would be lost to the atmosphere. The surface temperature is monitored at the steady-state condition using four thermocouples, which probe different locations of the chip. Knowing the average surface temperature and the heat flux supplied, the average heat transfer coefficient for heat loss is obtained. This heat transfer coefficient in combination with the measured surface temperature for a given experimental run is used for subtracting the heat loss.

2.2. Experimental Setup

The schematic of the experimental setup is shown in Figure 1. The test section consists of the microchannel with a serpentine heater integrated on the back side of the silicon wafer. Heat is supplied by a DC power source (Keithley Sourcemeter, 2400 series). Deionised water is used as the working fluid; the water is vigorously boiled and then cooled to room temperature to remove dissolved air. The water is pumped through a peristaltic pump

(Masterflex Easyflow II EW-77200-50) at a predetermined flow rate which is maintained constant for a given data point. The flow rate through the system is given by the pump itself and has a range of 0.1-6 ml/min. The flow rate was independently checked by measuring the mass of the water collected over 10 minutes duration and weighed on a microbalance.

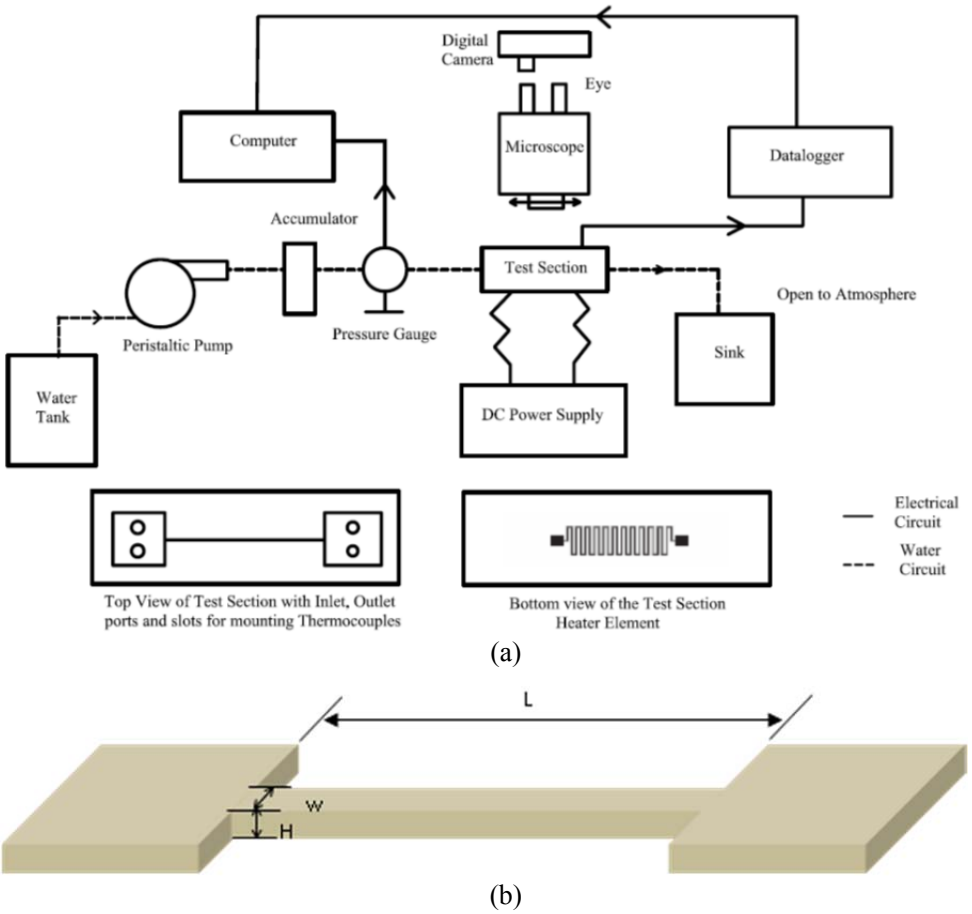

Figure 1. (a) Schematic of the experimental setup along with top and bottom view of the microchannel test section, (b) 3D view of microchannel geometry showing the measured geometrical parameters.

The microchannel has four ports, two at the inlet and two at the outlet. Two of these serve as entry and exit ports for the working fluid, and the remaining two are for inserting thermocouples (bead size of 0.5 mm, measurement accuracy ±1 K, response time of 10 ms). Three equally-spaced K-type thermocouples (bead size 25 μm, measurement accuracy of ±1 K, and response time of 1 ms) probe the surface temperature along the length of the microchannel. All the thermocouples used are connected to a data logger (Graphtec GL450) which collects data at 10 Hz frequency. A pre-calibrated digital pressure gauge (Keller, Leo 1 with a range of -1 to 3 bar, resolution of 0.05% of full scale, response time of 1 s) is connected at the inlet of the microchannel and provides the overall pressure drop (note that the pressure at the exit of the microchannel is atmospheric). The microchannel is oriented horizontally. The uncertainty in the different quantities, both measured and derived, is

provided in Table 1. The experimental setup has been carefully validated as discussed elsewhere [5, 12].

Table 1. Uncertainty for various parameters measured in the experiment

Parameter	Maximum error
Q	0.01 ml/min
L	100 μm
W	0.5 μm
H	0.5 μm
P	0.02 W
T	0.5 ºC
ΔP	2 mbar
A_{Ch}	1.49 %
d_h	1.87 %
q"	5.54 %
P_{chan}	5.42 %

The following procedure is adopted for performing the experiments. The water reservoir is filled with de-gassed, deionized water and the micro-pump is set for the desired flow rate. The pressure drop, temperature of inlet and outlet, and flow rate values are measured simultaneously using the data logger. The pressure drop across the entire microchannel is measured, which includes entry and exit losses. The pressure drop due to expansion and contraction (at the entry and exit) is however estimated to be negligibly small (0.3%) as compared to the overall pressure drop. The microheater dc power supply was set for a predetermined heat flux value. The experiment is then repeated for different flow rates and heat fluxes. The experiments have been carried out on a single microchannel of different hydraulic diameters (65, 70, 107, and 125 μm) and 2 cm length. The flow rate has been varied from 0.1-0.5 ml/min corresponding to mass flux values of 60-1410 kg/m^{2}s. The power supplied is in the range of 0-7 W (q" = 0-91 W/cm^2). The maximum exit quality in these experiments is 0.6.

2.3. Data Reduction

Data like input power, inlet/outlet temperature, and mass flow rate obtained through measurement has been processed using following approach. Water enters the inlet reservoir at atmospheric temperature and gets heated. The power used to heat water in reservoir is:

$$P_{reservoir} = \dot{m} C_p \left(T_{in} - T_{amb} \right) . \tag{1}$$

The heat gained by water at the inlet reservoir needs to be subtracted from the supplied power. This supplied power is directly obtained from the source meter. Therefore, power supplied to heat water in microchannel is given as,

$$P_{channel} = P_{supplied}(1-\lambda) - P_{reservoir} \tag{2}$$

where, λ is the percentage of heat loss to the atmosphere. Microheater fabricated on the back side of the microchannel is uniformly distributed along the microchannel length. Therefore, Power per unit length of microchannel is given as,

$$q^{'} = \frac{P_{channel}}{l}. \tag{3}$$

The heat input to the microchannel is utilised for both sensible and latent heating of water. Thus, energy balance of the system gives the thermodynamic quality as,

$$x = \frac{q^{'}l - \dot{m}C_p\left(T_{sat} - T_{in}\right)}{h_{fg}\dot{m}} \tag{4}$$

Heat flux supplied to the microchannel is given

$$q^{''} = \frac{P_{channel}}{A_s} \tag{5}$$

where, A_s is the sum of the areas of side walls and the bottom wall. Mass flux is given as,

$$G = \frac{\dot{m}}{A_c} \tag{6}$$

where, A_c is the cross-sectional area of the microchannel.

3. ONSET OF NUCLEATE BOILING (ONB)

Apart from the pressure drop and heat transfer characteristics, the onset of nucleate boiling (ONB) and critical heat flux (CHF) are other two important parameters of concern to a thermal engineer.

The ONB point is basically the heat flux at which the bubble nucleation is initiated in the microchannel. In most cases subcooled boiling leads to ONB. The phenomenon of ONB is important because it marks an abrupt change from single phase flow to two phase flow. It is therefore the lower limit for heat sinks operating in two-phase regime and the upper limit for single-phase heat sinks.

3.1. Technique for Measurement of ONB

In these experiments, the onset of nucleate boiling was determined from the change in the slope of the pressure drop versus heat flux curves. These curves are for a fixed value of mass flow rate. In single phase, the pressure drop decreases with an increase in heat flux, which is due to reduction in viscosity of water with temperature. Upon ONB, bubbles appear along the microchannel length which leads to an increase in the overall pressure drop. Thus, the point of change of slope in the pressure drop versus heat flux curve is taken as the point of ONB (Figure 2). ONB can also be obtained from the boiling curves. The first change in slope of the boiling curve signifies the ONB point. The point from boiling curve agrees with data obtained independently from the pressure drop curves for all the cases (not shown).

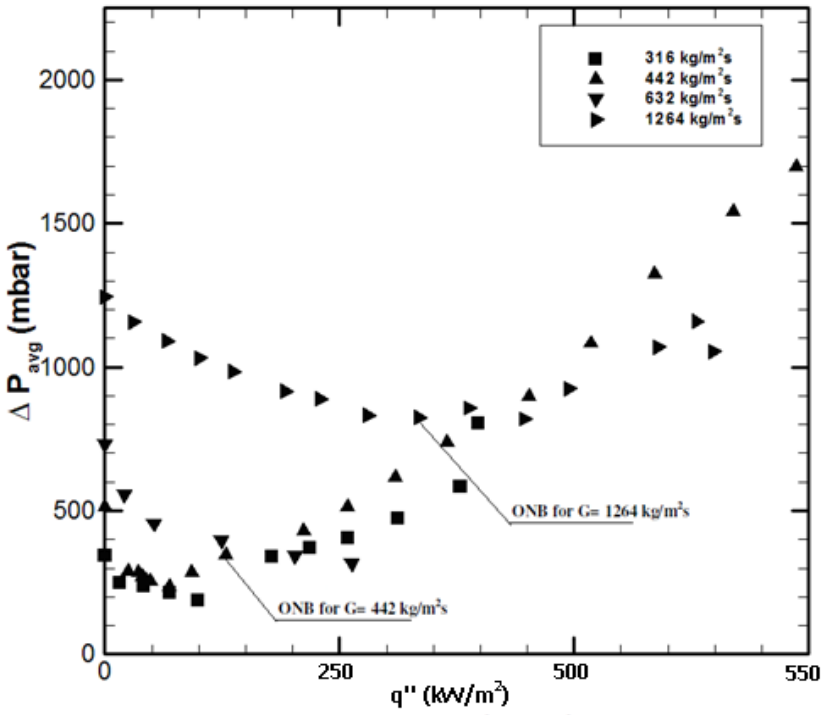

Figure 2. Variation of experimental pressure drop for different flow rates for 65 μm channel.

Figure 3 shows the variation of the ONB obtained experimentally with mass flux, in three different hydraulic diameter microchannels. For a given microchannel, the heat flux for ONB increases with an increase in mass flux, as expected. The heat flux required for ONB also increases with an increase in hydraulic diameter, for the same mass flux.

3.2. Comparison with ONB Correlations

The heat fluxes for ONB obtained experimentally are compared with different correlations. The comparison of the current dataset is limited to the correlations of Bergles

and Rohsenow [23] and Thom et al. [24]; these correlations are presented in Table 2. The heat flux required for ONB based on energy consideration, with T_{sat} = 100°C is calculated as,

$$q''_{boil} = \dot{m} C_p (T_{sat} - T_{in}) / A_h \,. \tag{7}$$

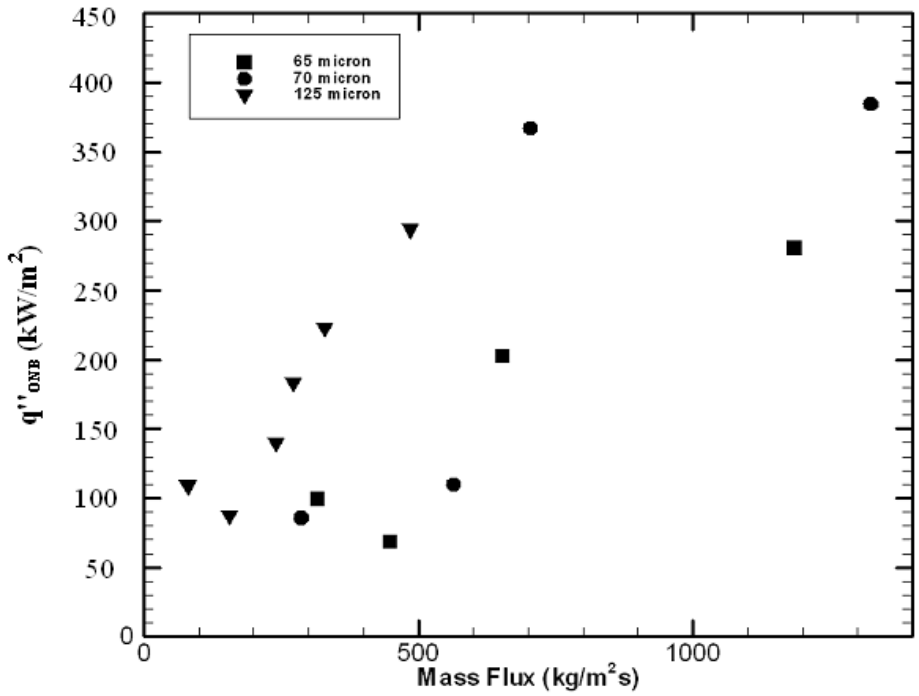

Figure 3. Variation of ONB with mass flux for different hydraulic diameters.

Note that most of the correlations for ONB are based on the work of Hsu [25]. The subsequent models of Sato and Matsumara [26], Davis and Anderson [27] and Kandlikar et al. [28] are of similar form but with a change in the empirical constants. These additional correlations were also tested in this work but were found to substantially over-predict most of the data-points; hence comparison with these correlations is not included here.

The comparisons with the aforementioned correlations are presented through Figs. 4, 5 and 6. Note that ratio of $q''_{predicted}$ to $q''_{experimental}$ as a function of mass flux is presented in the figures. The variation is largest with respect to the correlation of Thom et al. [24] (Figure 5). The correlation of Bergles and Rohsenow [23] also tends to over-predict the data (Figure 4). A relatively better match with the data (with most of the points lying within $\pm$ 50%) is found while comparing with q''_{boil} (Figure 6). On the whole, heat flux for ONB is predicted better at higher mass fluxes. Among all the correlations tested in this study, the simple energy balance calculation provides the best prediction. From Figs. 4-6 we note that the data for 125 μm channel is consistently over predicted by Thom et al. correlation as well as energy balance; but the energy balance method seems to fare better. For the 65 and 70 μm channel, Thom et al. correlation as well as energy balance under predicts the data. While simple energy balance show better prediction of ONB with increasing mass fluxes, Thom's correlation shows a

decreasing trend for $\frac{q''_{predicted}}{q''_{Expt}}$ with increasing mass flux. Interestingly, the correlation of Bergles and Rohsenow also shows a decreasing trend for $\frac{q''_{predicted}}{q''_{Expt}}$ with increased mass fluxes and the ratio approaches unity for higher mass fluxes.

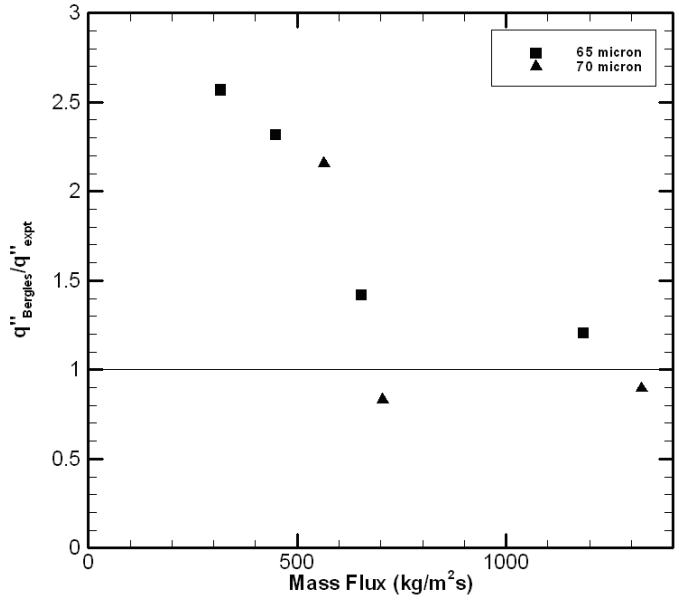

Figure 4. Comparison of ONB with the correlation of Bergles and Rohsenow [23].

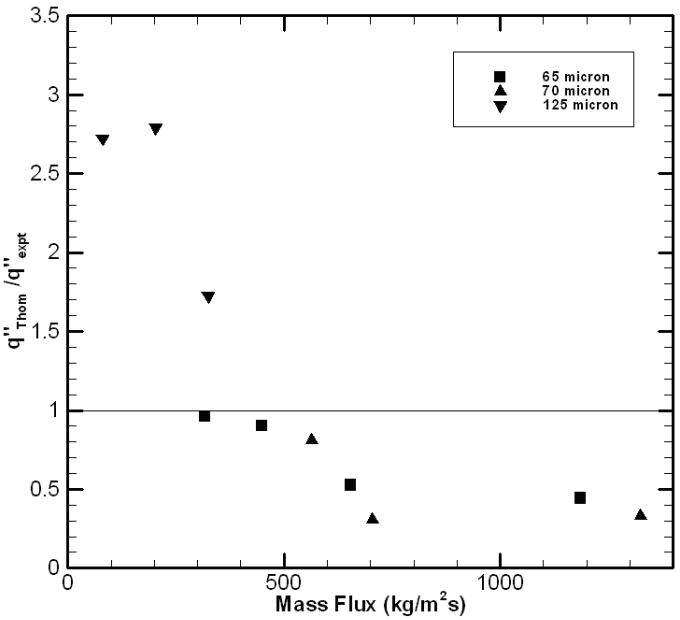

Figure 5. Comparison of ONB with the correlation of Thom et al. [24].

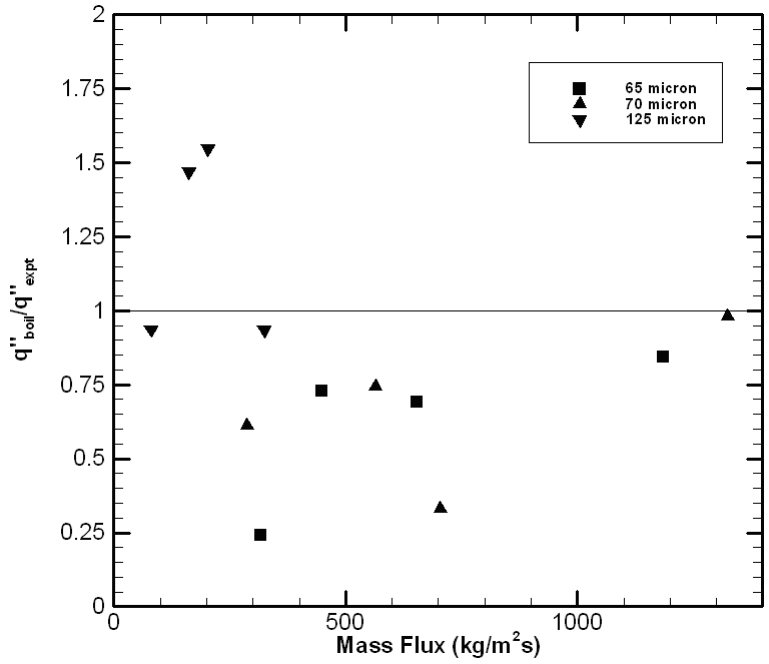

Figure 6. Comparison of ONB with $q"_{boil.}$

4. CRITICAL HEAT FLUX

Before moving on to the experimentally obtained CHF data (in Section 4.3), the procedure for determining CHF is discussed briefly in Sections 4.1 and 4.2.

4.1. CHF from Boiling Curves

CHF is estimated by plotting the boiling curve (heat flux versus surface temperature) (Figure 7a). While the first change in slope of the boiling curve indicates transition from single-phase to two-phase, the second change in slope occurs when the surface temperature increases rapidly owing to a drastic reduction in heat transfer coefficient. Thus, CHF corresponds to the point with a rapid increase in surface temperature.

Note that the two phase flow is accompanied by oscillations in temperature and pressure. From temperature-time plot, maximum, minimum and average temperatures can be determined. For example, in several cases the average surface temperatures may not be high (105-120 ^{o}C) while the peak temperatures may reach anywhere from 140-150 ^{o}C. Boiling curves with heat flux versus the maximum, minimum and average temperature are plotted and evaluated in Figure 7b. The figure shows that the CHF point is clearly obtained from plot of the maximum and average surface temperatures, while it is not so clear from the minimum temperature curve.

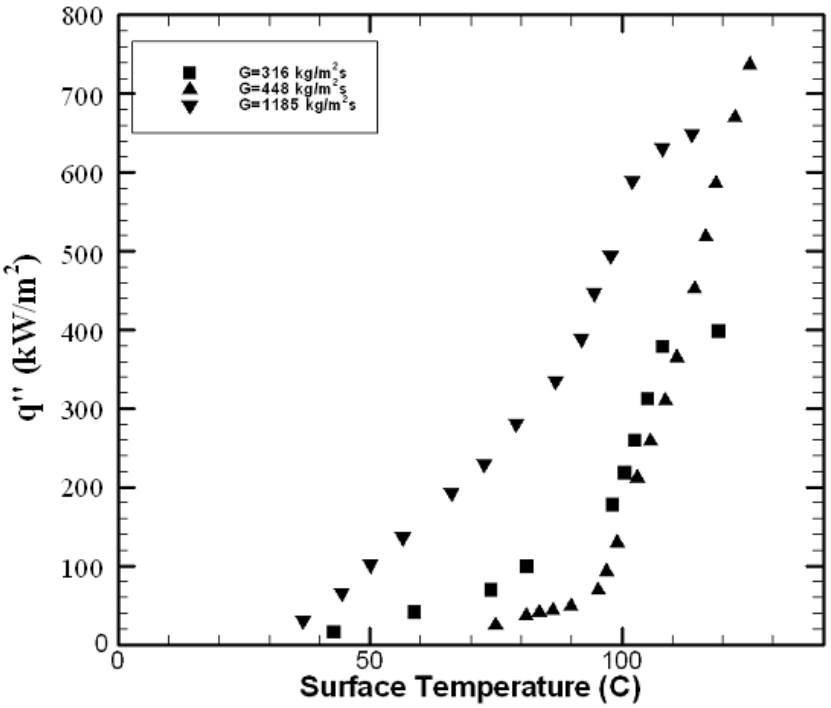

(a)

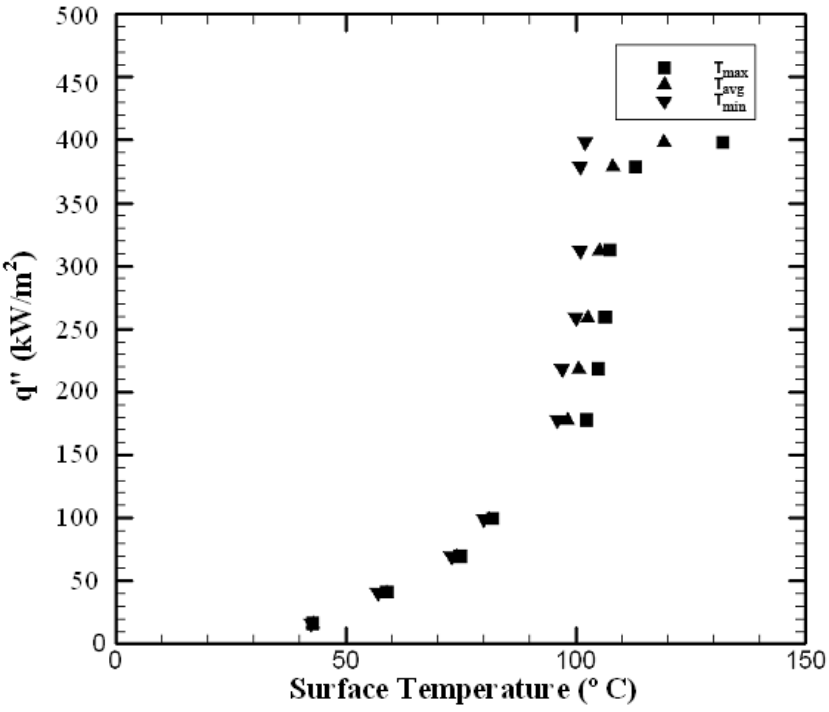

(b)

Figure 7. Boiling curve for 65 micron channel with (a) different mass flux values and (b) G = 316kg/m^{2}s with maximum, minimum and average temperatures.

4.2. CHF from Pressure Drop Curves

In these set of experiments, the heat flux is kept constant while the mass flux is systematically reduced. The curve shown in Figure 8a shows the typical variation of pressure drop [5]. The flow is initially in single phase region, which is represented by stars; with a reduction in flow rate the flow starts to boil, depicted by squares. The reason for this variation is discussed in sufficient detail in Singh et al. [5]. The heat flux corresponding to the sudden increase in pressure drop (point 'e' in Figure 8a) can be regarded as CHF for the particular value of mass flow rate. Note that the flow exhibits instability (i.e. the pressure varies rapidly with time). Singh et al. [5] and Bhide et al. [12] have quantified the variation in pressure with exit quality. In the former study, the normalized pressure (r.m.s. pressure by mean pressure) was found to be up to 14%. Further, the local maxima/ minima in normalized pressure were found to correlate very well with transitions in flow regime.

The above result is for a single heat flux value; a family of such curves was obtained, as shown in Figure 8b. The data obtained by Singh et al. [5] is unique because such detailed measurements on pressure drop, covering single-phase liquid, two-phase liquid-vapour and extending to dryout, are not available. In particular, Bergles and Kandlikar [29] have mentioned the difficulty in performing measurements in the regime d-e (in Figure 8a), highlighting that there is paucity of such data at the microscales. The CHF (estimated from point 'e') is influenced by the instabilities as pointed out by Bergles and Kandlikar [29]. It was specifically pointed out that microchannels with vaporization are prone to excursive instability which results in a relatively smaller value of CHF.

4.3. CHF Data and Comparison with Correlations

Note that instabilities are inherent in two-phase flow and no explicit attempt to suppress them has been made in this work. Quantification and discussion on the observed instabilities are provided elsewhere [5, 12]. The values reported here are therefore only indicative of the actual CHF.

The experimental CHF data points were obtained from one of the two methods discussed above (but not both) and plotted in Figure 9. Note that data from four different size microchannels is plotted in the figure. The CHF value increases with an increase in the mass flux (other than for d_h = 125 μm case). For a given mass flux value, the CHF appears to increase with a decrease in hydraulic diameter. Note that the surface roughness of 65 and 70 μm microchannels at ε/d_h = 0.0018 and 0.0171, respectively, are different by approximately an order of magnitude [12]. However, the effect of surface roughness with approximately the same hydraulic diameter microchannel is not reflected in the CHF values. This may be owing to the fact that CHF occurs due to DNB (formation of vapour blanket) – as indicated by low quality values. The vapour layer may be such that it is thicker than the roughness elements on the tube surface, thereby masking the effect of surface roughness. Chandraker et al. [22] correlated the CHF data from the literature (at 9660 data points) to the underlying flow regime. They found that the CHF generally increases with mass flux in the churn/slug region; however, the CHF decreases with increase in mass flux in the annular region. The increase in CHF is attributed to the enhanced level of turbulence in the churn flow regime as the flow

rate is increased; this delays the occurrence of CHF [22]. On the other hand, in the annular flow regime the dryout mechanism is dictated by the entrainment and deposition of droplets on the liquid film. At higher flow rate in the annular regime the rate of droplet entrainment due to shearing at the liquid film-vapor interface increases, this causes early dryout and lower CHF values.

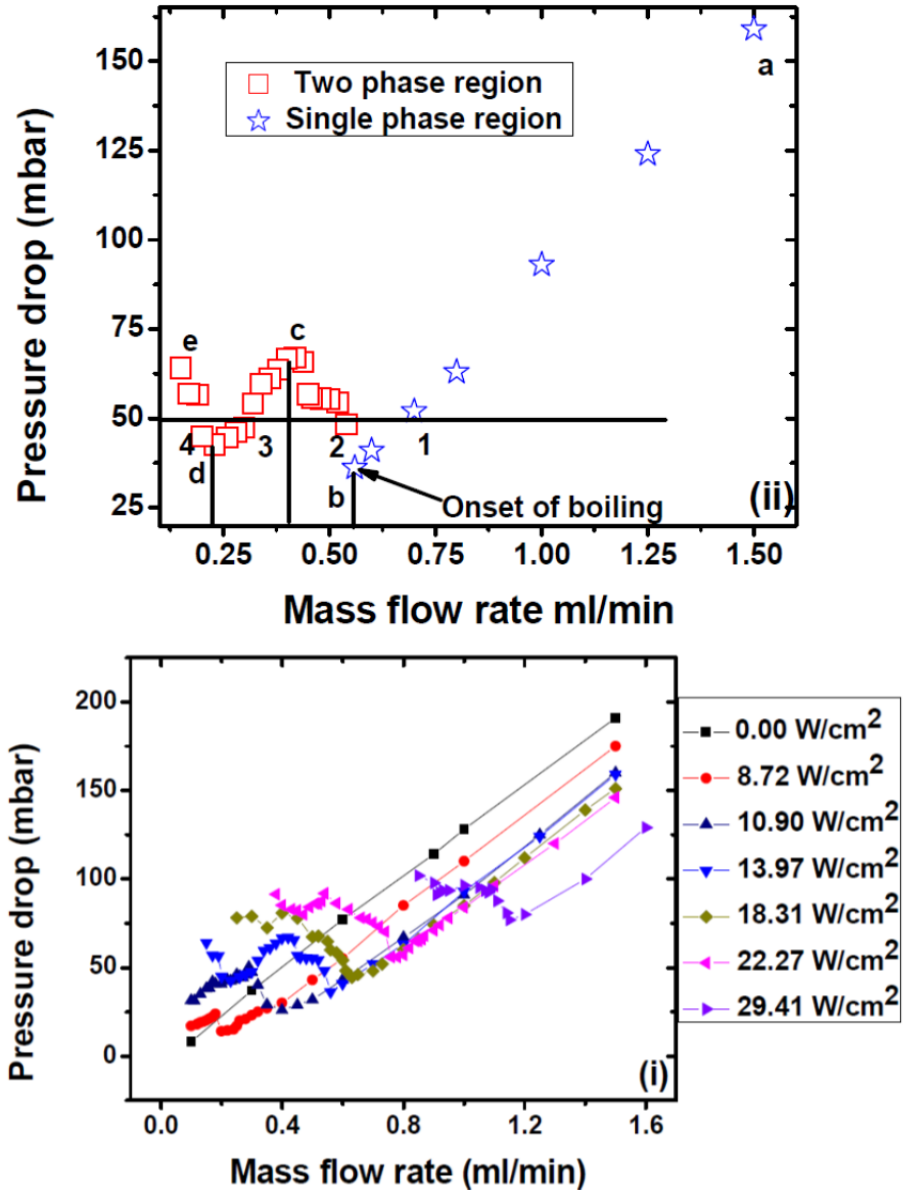

Figure 8. Experimental pressure drop versus mass flow rate for (a) heat flux of 13.97 W/cm^2 and (b) family of heat fluxes [5].

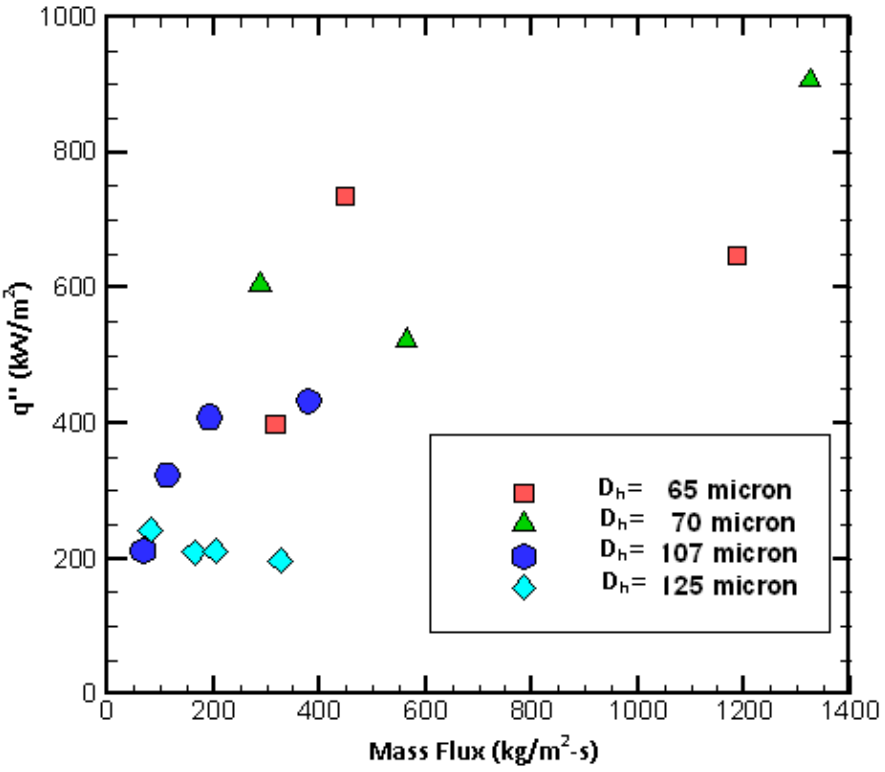

Figure 9. CHF versus mass flux.

Table 2. Correlations used for comparison with ONB

Bergles and Rohsenow [23]	$q''_{ONB} = 1082 P_{sat}^{1.156} \left[1.8\left(T_w - T_{sat}\right)\right]^{2.16/P_{sat}^{0.0234}}$; P_{sat} in bar, q"$_{ONB}$ in MW/m^2
Thom et al. [24]	$q''_{ONB} = \left[\dfrac{\Delta T_{sat}}{22.65 \exp\left(-P_{sat}/87\right)}\right]^2$; P_{sat} in bar; q"$_{ONB}$ in MW/m^2
Single phase energy balance, q"$_{boil}$	$q''_{boil} = \dfrac{\dot{m} C_p \left(T_{sat} - T_{in}\right)}{A_h}$, T_{sat} = 100°C

Figure 9 shows an increasing trend in CHF with mass flux for all microchannels (other than 125 μm). The flow regime is however believed to be annular in all the cases [5, 12]. The result therefore suggests a change in the mechanism leading to CHF at the micro-scales. The mechanism of CHF is yet to be fully understood and calls for further detailed investigations.

Table 3. Correlations used for comparison with CHF

Qu and Mudawar [14]	$q''_{CHF} = 33.43 G h_{fg} \left(\frac{\rho_g}{\rho_f}\right)^{1.11} We^{-0.21} \left(\frac{L}{d_h}\right)^{-0.36}$
Katto [30]	$q''_{CHF} = q''_{CHF,0}\left(1 + K\frac{\Delta h_{sub,in}}{h_{fg}}\right)$ $q''_{CHF,1} = 0.25\left(Gh_{fg}\right)\frac{1}{L/d_h}$ $q''_{CHF,2} = C\left(Gh_{fg}\right)We^{-0.043}\frac{1}{L/d_h}$ $q''_{CHF,3} = 0.15\left(Gh_{fg}\right)\left(\frac{\rho_g}{\rho_f}\right)^{0.133} We^{-1/3}\frac{1}{1+0.0077\,L/d_h}$ $q''_{CHF,3} = 0.26\left(Gh_{fg}\right)\left(\frac{\rho_g}{\rho_f}\right)^{0.133} We^{-0.433}\frac{\left(L/d_h\right)^{0.171}}{1+0.0077\,L/d_h}$ C=0.25 for $L/d_h < 50$; C= 0.34 for $L/d_h > 50$ $K_1 = 1$; $K_2 = \frac{0.261}{CWe - 0.043}$; $K_3 = \frac{0.556\left(0.0308 + d_h/L\right)}{\left(\rho_g/\rho_f\right)^{0.133} We^{-1/3}}$ $q''_{CHF,1} < q''_{CHF,2}$; $q''_{CHF,0} = q''_{CHF,1}$; $K = K_1$ $q''_{CHF,1} > q''_{CHF,2}$; *if* $q''_{CHF,2} < q''_{CHF,3}$; $q''_{CHF,0} = q''_{CHF,2}$; $K = K_2$ $q''_{CHF,2} > q''_{CHF,3}$; *if* $q''_{CHF,3} < q''_{CHF,4}$; $q''_{CHF,0} = q''_{CHF,3}$; $K = K_3$ $q''_{CHF,3} > q''_{CHF,4}$; $q''_{CHF,0} = q''_{CHF,4}$
Mishima and Ishii [31]	$q''_{CHF} = \frac{A_{cross}}{A_h} h_{fg}\left[\frac{G\Delta h_{sub,in}}{h_{fg}} + \left(\frac{1}{Co} - 0.11\right)\sqrt{\rho_g g(\rho_f - \rho_g) d_h}\right]$ $Co = 1.35 - 0.35\sqrt{\frac{\rho_g}{\rho_f}}$
Sudo et al. [32]	$q''_{CHF} = 0.005 h_{fg} G^{0.611}\left[\lambda\rho_g g(\rho_f - \rho_g)\right]^{0.195}$ $\lambda = \sqrt{\frac{\sigma}{(\rho_f - \rho_g)g}}$

Table 4. Comparison of $q"_{max}$ (expt) with different CHF correlations for various hydraulic diameters

Case I: Hydraulic diameter = 65 micron

Sr. No.	G (kg/m^2s)	Expt	Comparison with Correlations				Exit qlty	$q"_{max}/q"_{Mu}$
		$q"_{max}$ (kW/m^2)	$q"_{chf}$ (kW/m^2) (Katto)	$q"_{chf}$ (kW/m^2) (Mishima)	$q"_{chf}$ (kW/m^2) (Sudo)	$q"_{chf}$ (kW/m^2) (Mudawar)		
1	316	398	668	152	637	398	0.37	1.00
2	448	736	672	224	788	488	0.55	1.51
3	1185	648	652	465	143	858	0.16	0.76

Case II: Hydraulic diameter = 70 micron

Sr. No.	G (kg/m^2s)	Expt	Comparison with Correlations				Exit qlty	$q"_{max}/q"_{Mu}$
		$q"_{max}$ (kW/m^2)	$q"_{chf}$ (kW/m^2) (Katto)	$q"_{chf}$ (kW/m^2) (Mishima)	$q"_{chf}$ (kW/m^2) (Sudo)	$q"_{chf}$ (kW/m^2) (Mudawar)		
1	287	605	630	122	600	385	0.63	1.57
2	564	524	627	228	907	570	0.26	0.92
3	1324	907	610	450	1528	935	0.15	0.97

Case III: Hydraulic diameter = 107 micron

Sr. No.	G (kg/m^2s)	Expt	Comparison with Correlations				Exit qlty	$q"_{max}/q"_{Mu}$
		$q"_{max}$ (kW/m^2)	$q"_{chf}$ (kW/m^2) (Katto)	$q"_{chf}$ (kW/m^2) (Mishima)	$q"_{chf}$ (kW/m^2) (Sudo)	$q"_{chf}$ (kW/m^2) (Mudawar)		
1	67	212	228	49	246	193	0.37	1.10
2	111	324	378	79	336	260	0.34	1.24
3	191	409	650	132	468	356	0.20	1.15
4	378	434	1270	232	710	529	0.07	0.82

Case IV: Hydraulic Diameter = 125 micron

Sr. No.	G (kg/m^2s)	Expt q''_{max} (kW/m^2)	Comparison with Correlations q''_{chf} (kW/m^2) (Katto)	q''_{chf} (kW/m^2) (Mishima)	q''_{chf} (kW/m^2) (Sudo)	q''_{chf} (kW/m^2) (Mudawar)	Exit qlty	q''_{max}/q''_{Mu}
1	81	243	307	33	277	226	0.47	1.08
2	163	210	623	72	424	338	0.20	0.62
3	203	212	775	86	486	385	0.16	0.55
4	325	197	1211	109	648	505	0.06	0.39

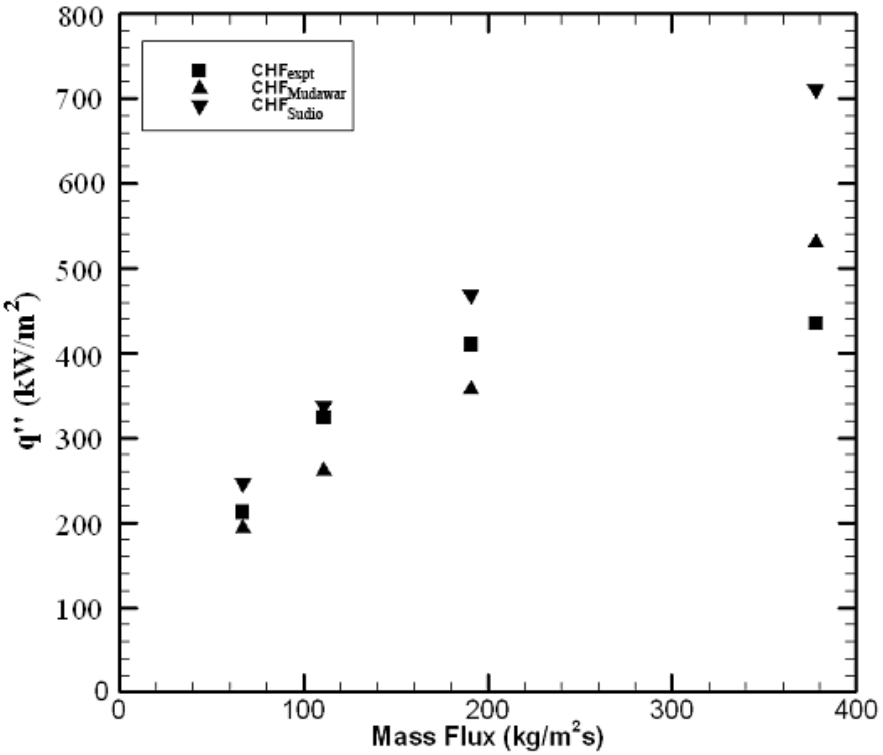

Figure 10. Comparison of CHF with the correlation of Sudo et al. [32] and Qu and Mudawar [14] for 107 μm channel.

The CHF value obtained experimentally is compared with the correlations of Katto [30], Mishima and Ishii [31], Sudo et al. [32] and Qu and Mudawar [14]. These correlations are tabulated in Table 3. Figure 10 and Table 4 provide a comparison of predicted and experimental values. Of the correlations tested, the correlation of Qu and Mudawar is for microscales while the other correlations are for conventional (macro) scale. It is seen from Table 4 that the CHF values obtained from the correlation of Qu and Mudawar compares with the experimental data better than the other tested correlations. In general, the correlation of Katto over-predicts the CHF data, while the correlation of Mishima under-predicts. A similar observation has been reported by Qu and Mudawar [14]. The correlation of Sudo et al. predicts the CHF data reasonably well; this correlation was however developed for flow in vertical rectangular channels.

DISCUSSION AND CONCLUSION

Experimental heat flux values for onset of nucleate boiling and critical heat flux are reported in this paper, as a function of mass flux and hydraulic diameter. The primary goal of this work is to add data points to the existing literature on microchannels, so that a more appropriate correlation for CHF at the microscales can eventually emerge. The obtained range of ONB and CHF are 50-400 kW/m^2 and 200-900 kW/m^2, respectively, with hydraulic diameter in the range of 65-125 μm and mass flux in the range of 60-1410 kg/m^2-s. The CHF

is obtained from the boiling curve where a distinct increase in surface temperature occurs for a comparatively small increase in the applied heat flux. Alternatively, the CHF is obtained from the pressure drop curves in the two phase region, where backflow was observed. The CHF points are accompanied by fluctuations in pressure and temperature, and are responsible for premature CHF in microchannels. In several cases the average surface temperatures may not be high (105-120^{o}C) while the peak temperatures may reach anywhere from 140-150^{o}C. Such high temperatures though observed intermittently, can cause serious damage to the device.

Besides providing ONB and CHF data in extremely small channels, this paper also provides comparison with different correlations. In particular, the experimental CHF values are found to compare within $\pm 25\%$ with the correlation of Qu and Mudawar [14]. This correlation has been developed specially from microchannel database for CHF obtained from experiments done on water and R-113. It is needless to emphasize that the CHF data points are difficult to obtain and are rarely reported in the literature especially in the context of microchannels. The generation of CHF data is important as the occurrence of CHF is an important design consideration in two phase microchannel heat sinks. These results therefore provide useful lower and upper limits on heat flux to maintain two phase flow regime in microchannels.

ACKNOWLEDGMENTS

We are grateful to Mr. Anshul Jain for some initial calculations.

REFERENCES

[1] J.R. Thome, Boiling in microchannels: a review of experiment and theory, *Int. J. Heat and Fluid Flow* 25 (2004) 128-139.

[2] M Lee, Y. Y. Wong, M. Wong, Y. Zohar, Size and shape effects on two phase flow patterns in microchannel forced convection boiling, *Journal of Micromechanics and Microengineering,* 13 (2003) 155-164.

[3] W. Qu, I. Mudawar, Flow boiling heat transfer in two-phase micro-channel heat sinks––I. Experimental investigation and assessment of correlation methods, *Int. J. Heat Mass Transfer* 46 (2003) 2755-2771.

[4] L. Zhang, J.M. Koo, L. Jiang, M. Asheghi, K.E. Goodson, J.G. Santiago, T. W. Kenny, Measurements and modelling of two phase flow in microchannels with nearly constant heat flux boundary conditions, *J. Microelectromechanical Systems*, 11 (2002) 12-19.

[5] S.G. Singh, R. Bhide, B. Puranik, S.P. Duttagupta, A. Agrawal, Two-phase flow pressure drop characteristics in trapezoidal silicon microchannels, *IEEE Transactions of Components and Packaging Technology*, 32 (2009) 887-900.

[6] S. G. Singh, A. Jain, A. Sridharan, S. P. Duttagupta, A. Agrawal, Flow map and measurement of void fraction and heat transfer coefficient using image analysis technique for flow boiling of water in silicon microchannel, *J. Micromech. Microeng.,* 19 (2009) 075004.

[7] L. Jiang, M. Wong, Y. Zohar, Phase change in microchannel heat sinks with integrated temperature sensors, *J. of Microelectromechanical systems*, 8 (1999) 358-365.

[8] M.E. Steinke, S.G. Kandlikar, An Experimental Investigation of Flow Boiling Characteristics of Water in Parallel Microchannels, *Transactions of ASME*, 126 (2004), 518-526.

[9] G. Hestroni, A. Mosyak, E. Pogrebnyak, Z. Segal, Periodic boiling in parallel micro-channels at low vapour quality, *Int. J. Multiphase flow,* 32 (2006) 1141-1159.

[10] H.Y. Wu and P. Cheng, Boiling instability in parallel silicon microchannels at different heat flux, *Int. J. of Heat and Mass Transfer*, 47 (2004), 3631-3641.

[11] G. Hetsroni, A. Mosyak, E. Pogrebnyak, Z. Segal, Explosive boiling of water in parallel micro-channels, *Int. J. Multiphase Flow*, 31 (2005) 371-392.

[12] R.R. Bhide, S.G. Singh, A. Sridharan, S.P. Duttagupta, A. Agrawal, Pressure drop and heat transfer characteristics of boiling water in sub-hundred micron channel, *Experimental Thermal and Fluid Science,* 33 (2009) 963-975.

[13] S.G. Singh, A. Kulkarni, S.P. Duttagupta, B.P. Puranik, A. Agrawal, Impact of aspect ratio on flow boiling of water in rectangular microchannels, *Experimental Thermal and Fluid Science* 33 (2008) 153–160.

[14] W. Qu, I Mudawar, Measurement and correlation of critical heat flux in two-phase micro-channel heat sinks, *International Journal of Heat and Mass Transfer* 47 (2004) 2045–2059.

[15] L. Wojtan, R. Revellin, J.R. Thome, Investigation of saturated critical heat flux in a single, uniformly heat microchannel, *Experimental Thermal and Fluid Science*, 30 (2006) 765-774.

[16] J. Lee, I. Mudawar, Critical heat flux for subcooled flow boiling in micro-channel heat sinks, *International Journal of Heat and Mass Transfer*, 52 (2009) 3341-3352.

[17] Kosar, and Y. Peles, Critical Heat Flux of R-123 in Silicon-Based Microchannels, *Journal of Heat Transfer,* 129 (2007) 844-851.

[18] W.K. Kuan, and S.G. Kandlikar, Experimental Study and Model on Critical Heat Flux of Refrigerant-123 and Water in Microchannels, *Journal of Heat Transfer*, 130 (2008) 034503.

[19] A.P. Roday, and M.K. Jensen, Study of the Critical Heat Flux Condition with Water and R-123 During Flow Boiling in Microtubes. Part I: Experimental Results and Discussion of Parametric Effects, *Int. J. Heat Mass Trans*., 52 (2009) 3235-3249.

[20] Kosar, A model to predict saturated critical heat flux in minichannels and microchannels. *Int. J. of Thermal Sciences* 48 (2009) 261-270.

[21] P.U. Patankar, B.P. Puranik, Modifications and extensions to the annular flow model, in Proceedings of the Fourth International Conference on Nanchannels, Microchannels, and Minichannels, Limerick, Ireland, ICNMM2006-96053 (2006).

[22] D.K. Chandraker, P.K. Vijayan, D. Saha and R.K. Sinha, Investigation on the characteristic of CHF in various flow pattern regimes based on look-up table data, *Nuclear Engineering Design,* 238 (2008), 170–177.

[23] A.E. Bergles, W.M. Rohsenow, The determination of forced-convection surface-boiling heat transfer, *J. Heat Transfer* 86 (1964) 365–372

[24] J.R.S. Thom, W.M. Walker, T.A. Fallon, and G.F.S. Reising, Boiling in subcooled water during flow up heated tubes or annuli. Symposium on Boiling Heat Transfer in

Steam Generating Units and Heat Exchangers, Manchester, 15-16 September 1965. IMechE, London (1965).

[25] Y.Y. Hsu, On the size range of active nucleation cavities on a heating surface, *J. Heat Transfer* 84 (1962) 207–216.

[26] T. Sato, H. Matsumura, On the conditions of incipient subcooled-boiling with forced convection, Bull. *JSME* 7 (1963) 392–398.

[27] E.J. Davis, G.H. Anderson, The incipience of nucleate boiling in forced convection flow, *AIChE J*. 12 (1966) 774–780.

[28] S.G. Kandlikar, V. Mizo, M. Cartwright, E. Ikenze, Bubble nucleation and growth characteristics in subcooled flow boiling of water. National Heat Transfer Conference, HTD-342, *ASME*, 1997, 11–18.

[29] E. Bergles, S.G. Kandlikar, On the Nature of Critical Heat Flux in microchannels, *J. Heat Transfer* 127 (2005) 101-107.

[30] Y. Katto, General features of CHF of forced convection boiling in uniformly heated rectangular channels, *Int. J. Heat Mass Transfer* 24 (1981) 1413–1419.

[31] K. Mishima, M. Ishii, Critical heat flux experiments under low flow conditions in a vertical annulus, ANL-82-6, NUREG/CR-2647, 1982.

[32] Y. Sudo, K. Miyata, H. Ikawa, M. Kaminaga, M. Ohkawara, Experimental study of differences in DNB heat flux between upflow and downflow in vertical rectangular channel, *J. Nucl. Sci. Technol*. 22 (1985) 604–618.

[33] N. Basu, G. R. Warrier, V. K. Dhir, Onset of nucleate boiling and active nucleation site density during subcooled flow boiling, *Journal of Heat Transfer* 124 (2002) 717-728.

[34] W. Qu, I. Mudawar, Prediction and measurement of incipient boiling heat flux in micro-channel heat sinks, *International Journal of Heat and Mass Transfer*, 45 (2002), 3933-3945.

[35] D. Liu, P. Lee, S. V. Garimella, Prediction of the onset of nucleate boiling in microchannel flow, *International Journal of Heat and Mass Transfer*, 48 (2005), 5134-5149.

[36] Agrawal, S.G. Singh, A review of state-of-the-art on flow boiling of water in microchannel, *International Journal of Microscale and Nanoscale Thermal and Fluid Transport Phenomena,* 2 (2011) 1-39.

[37] S.G. Singh, R.R. Bhide, S.P. Duttagupta, A. Sridharan, A. Agrawal, Experimental study of water boiling in microchannel, Advances in Multiphase Flow and Heat Transfer, Eds: L. Cheng and D. Mewes, Vol. 3, pp. 246-303, Chapter 6, 2010 (Bentham Science Publishers).

Received 03 October 2011, *received* in revised form 12 August 2012; *accepted* 18 August 2012.